Mechanical Deformation of Nanoscale Metal Rods: When Size and Shape Matter

M. J. Lagos,[1,2] F. Sato,[3] D. S. Galvão,[1] and D. Ugarte[1,*]

[1]*Instituto de Física "Gleb Wataghin," Universidade Estadual de Campinas-UNICAMP,*
Rua Sérgio Buarque de Holanda 777, 13083-859 Campinas SP, Brazil
[2]*Laboratório Nacional de Luz Síncrotron–LNLS, CP 6192, CEP 13083-970, Campinas–SP, Brazil*
[3]*Departamento de Física, ICE, Universidade Federal de Juiz de Fora, CEP 36036-330 Juiz de Fora–MG, Brazil*

Face centered cubic metals deform mainly by propagating partial dislocations generating planar fault ribbons. How do metals deform if the size is smaller than the fault ribbons? We studied the elongation of Au and Pt nanorods by *in situ* electron microscopy and *ab initio* calculations. Planar fault activation barriers are so low that, for each temperature, a minimal rod size is required to become active for releasing elastic energy. Surface effects dominate deformation energetics; system size and shape determine the preferred fault gliding directions which induce different tensile and compressive behavior.

PACS numbers: 62.25.−g, 61.46.−w, 68.37.Og

The mechanical properties of a strained nanoscale volume of matter represent a fundamental issue for understanding phenomena such as friction, fracture, etc. Miniaturization is raising the need for characterizing nanomaterials to develop models and predictions of their mechanical performance and reliability [1].

Concerning bulk matter, the mechanical behavior of face centered cubic (fcc) metals is one of the most studied cases, where deformation can be understood by the gliding of compact (1 1 1) atomic planes and the formation of an extended dislocation. In fact, a total dislocation (TD) is dissociated into two partial edge dislocations (PDs); this dissociation generates a stacking fault (SF) ribbon [2]. The ribbon width (d) is determined by an attractive force trying to minimize the area and a repelling force between the deformed PD regions. Several fcc metals (gold, silver, etc.) are soft and ductile due to the easy dislocation propagation [3].

When the size scale is reduced, the existence of a free surface modifies significantly the dislocation dynamics. *In situ* deformation of gold pillars (200–900 nm in diameter) in a scanning electron microscope [4,5] revealed that these pillars exhibit clear size effects. In fact, dislocations escape easily from the crystal through free surfaces, which induces a lack of strain hardening.

What will happen if we move to very tiny gold nanorods, where the diameter (~ 1 nm) is smaller than the SF ribbon width in bulk ($d \sim 3$ nm in bulk Au [3])? In this size regime, the plastic deformation description based on dislocation motion and SF ribbon can no longer be used anymore. In analogy, Luo *et al.* [6] have recently demonstrated that metallic glass rods, which are brittle in bulk, become ductile when their diameter is below their typical shear band size.

Force measurements have shown that elongation of Au nanorods (NRs) follows a series of elastic stages and sudden yielding points associated with structural

reorganization [7]. Insights into nanoscale deformation mechanisms [1,8,9] have been obtained from simulations, where the used time scales and deformation speeds are several orders of magnitude higher than in experiments [9–11]. The experimental validation is then seriously hindered, because temperature dependent effects and rate limited processes cannot be accounted for [9,11]. Here, we present a direct time-resolved and atomic resolution imaging study of temperature effects on the structural evolution of 1-nm-wide metal rods subjected to mechanical elongation. Our results show that surface energy overrules planar faults. System size and shape influence fault gliding directions which may induce different tension and compression behaviors.

The rods were generated *in situ* inside an atomic resolution electron microscope (HRTEM) (see videos in supplemental information [12]). This method does not allow us to either control the deformation or to measure applied forces [13]. Modern HRTEM sample holders allow controlled NR manipulation and the measurement of applied forces and transport properties [14–18]. Unfortunately, it is only possible to make studies at room temperature. The experiments discussed here have used a simple approach [13] in order to study NR stretching at different temperatures. Numerous events (more than 200 at 300 K and 100 at 150 K) were measured providing information at atomic level; the ensemble of experiments includes different elongation speeds, shear component contributions, apex atomic structure, etc.

Figure 1(a) shows some images of a 0.8 nm-wide Au NR being elongated at 300 K along the [1 1 0] direction (hereafter noted [1 1 0] rod). For a fcc metal stretched along the [1 1 0] direction, we expect the gliding of (1 1 1) and (1 1 −1) planes [2,3] [see Fig. 2(a), left side]. However, the NR stretched at 300 K seems to stay defect free and the rod breaks abruptly [19] (see supplemental information [12], video 01). Surface atoms easily diffuse
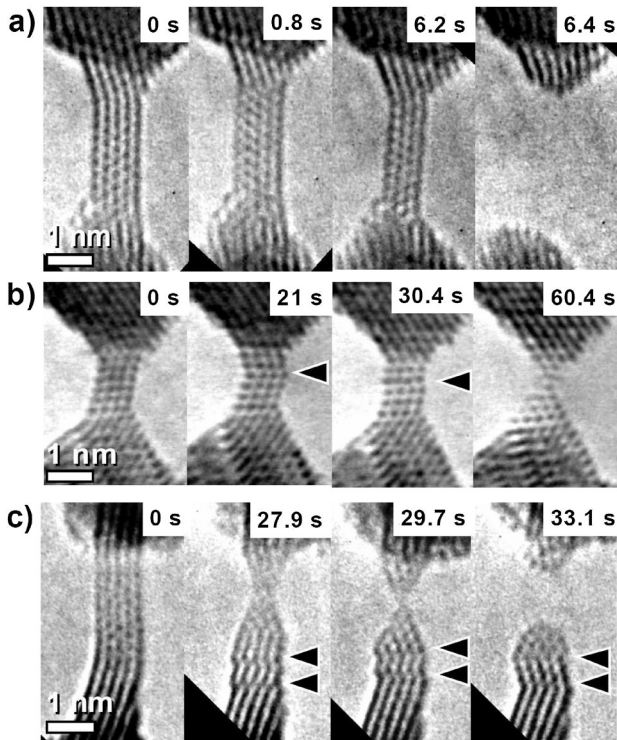
FIG. 1. Snapshots showing the elongation of Au nanorods along the [1 1 0] direction: (a) 300 K; (b) and (c) 150 K. Note that the structure seems to stay straight and defect free in (a), while the formation of structural planar defects can be easily identified in (b) and (c) (indicated by arrows). Elongation rates were ~0.02, ~0.03, and ~0.02 nm/s for (a), (b), and (c), respectively. Atomic positions appear dark.

FIG. 2. (a) Left side: scheme of the atomic arrangement of a [110] rodlike NW formed by 5 (200) atomic planes [Fig. 1(a) (0's)]; right side: expected cross section. (b) Top: scheme of a wire formed by 4 (−1 1 −1) planes [Fig. 1(b) (0's)], the ABC sequence of stacked hexagonal-close-packed planes is indicated. (b) Bottom: glide of one rod section over the 4th (111) atomic plane by a 1/6 [211] (generated planar defect is arrowed) and, glide by 1/2 [1 1 0] which generates a higher surface step but realigns the remaining (−1 1 −1) planes; at right, a twin defect (fifth layer) is exemplified (arrowed).

on the rod facets, moving towards the apexes at 300 K during the thinning process. At low temperatures [Figs. 1 (b) and 1(c); supplemental information [12], video 02 and video 03), the NR evolution is significantly modified with formation of planar defects, which represent a modification of the regular stacking sequence of compact (1 1 1) planes or more complex changes of the stacking sequences such as twins (TWs). Also, the rodlike wires form bipyramidal junctions before rupture, leading to the formation of suspended atomic chains [14,20]. In Figs. 1(b) and 1(c), the [1 1 0] NWs are observed along a different direction, the (1 1 1) slip planes appear horizontal in the images [see schematic drawing in Fig. 2(b)]. As predicted by simulations performed by Landman *et al.* [21], the planar defects in Figs. 1(b) and 1(c) correspond to the compact glide of the (1 1 1) planes by (1/6) [1 1 2]. This slip can be also interpreted on the basis of nanodisturbances as proposed by Bobylev *et al.* [22] for 1 nm-wide NR. In bulk, this glide generates Shockley PDs; in nanoscale rods, the glide of atomic plane generates surface steps that must represent a significant energy increase [Fig. 2(b)].

Our results have clearly identified two distinct structural behaviors during the deformation of nm-wide gold rods at 300 and 150 K. Using the crystallographic Wulff method [23,24], it is possible to demonstrate that the rods observed
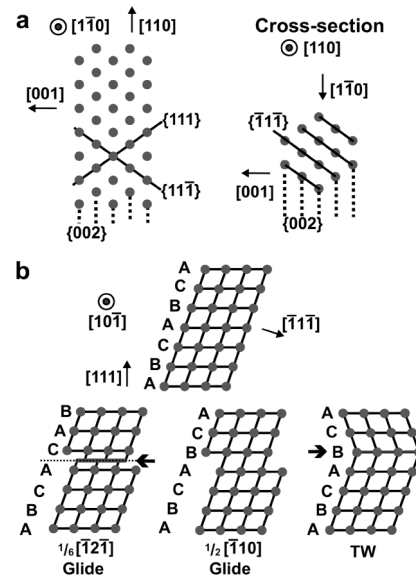
in Figs. 1(a) and 1(b) have exactly the same cross section (see Fig. 2 and supplemental information [12]). This allows a direct comparison between experiments realized at different temperatures. At 300 K and within our time resolution (33 ms), the 1-nm-wide rod seems to easily annihilate defects during deformation; in contrast, planar defects generated by compact glide of atomic planes are observable at 150 K. This suggests that, for Au rod of ~1 nm in diameter, thermal energy plays an essential role for defect annihilation. Applying the Arrhenius method, we can estimate the energy barrier (ΔE) associated with the whole atomic plane glide recombination. Unfortunately, due to experimental constraints, only two different temperatures are available as input data; analyzing the experimentally observed lifetimes, a barrier $\Delta E \sim 40$ meV is roughly estimated for a 1-nm gold rod (see supplemental information [12]). In principle, the barrier value should be considered size dependent (in first approximation proportional to NR cross section), because planar defects are bidimensional structural configurations whose energy contributions depend on their area. In fact, HRTEM observations indicate a relationship between energy barrier and NR size. For example, we have experimentally observed planar defects in thicker (~ 4 nm) Au NRs at room temperature; Kurui *et al.* [18] have also reported the observation of planar defects in 2.5 nm-wide gold rods at 300 K.

In order to further test a correlation between temperature and barrier height, we can perform experiments using

another fcc metal with different planar defect energetics. A point in case is Pt, because in bulk the barrier to glide one compact (1 1 1) atomic plane (Rice criteria [25,26]) is about twice the gold value [27,28]. Similar behavior should be expected if temperature is doubled (150 to 300 K). The images in Fig. 3(a) confirm the observation of planar defects during deformation of a Pt NR of similar size even at room temperature. Extending our interpretation, we should observe other defects with lower barriers at 150 K. In fact, Fig. 3(b) shows a Pt NR containing a grain boundary; a detailed analysis reveals that a defect such as a boundary dislocation exists at the center of the Pt NR. Similar formation and propagation of grain boundaries were observed in metallic nanocapsules under mechanical deformation [29].

We have performed *ab initio* calculations [30] to get further insights into the energetics of planar defect generation in NRs. We have calculated the total energy changes associated with the glide of one half of a NR over the other half. This is equivalent to calculate a generalized stacking fault surface for a macroscopic fcc system [2,3,25,27,28], but we are intrinsically incorporating the surface contribution. For the NR in Fig. 2(b), the (1 1 1) gliding planes display an elongated hexagonal shape [see Fig. 4(a)]. We have considered the whole atomic plane slip recovering the right stacking sequence of a fcc rod. We have generated the total slip displacement of the shortest lattice vector of type ([1 1 0]/2) by two successive glides of type [1 1 2]/6. These atomic plane glides are equivalent to the splitting of a TD into two Shockley PDs in bulk fcc metals [2,3].

Considering slip plane morphology, six possible final positions can generate a glide corresponding to a [1 1 0]/2 kind of vector; they can be grouped into three dissimilar configurations (indicated 1, 2, 3 in Figs. 4(a) and 4(b); pathways 2 and 3 share the first slip step). Path 1 should be induced by a tensile force, as the slip follows the projected shear force component. Path 2 requires an additional shear force in a direction perpendicular to a pure tensile effort; finally, path 3 represents a slip generated by compression (total displacement in opposite direction to path 1).

The nanorod total energy curves along the glide paths show somewhat two shallow bumps (associated with each slip step energy barrier) superimposed on an important background [Fig. 4(c)]. We deduce that the high background must be associated with the generation of surface steps. In fact, the barriers related to the glide of compact planes (bumps height) seem to be much less important than surface contribution in 1-nm-wide Au rods. As the surface contribution is always increasing along the slip direction, it
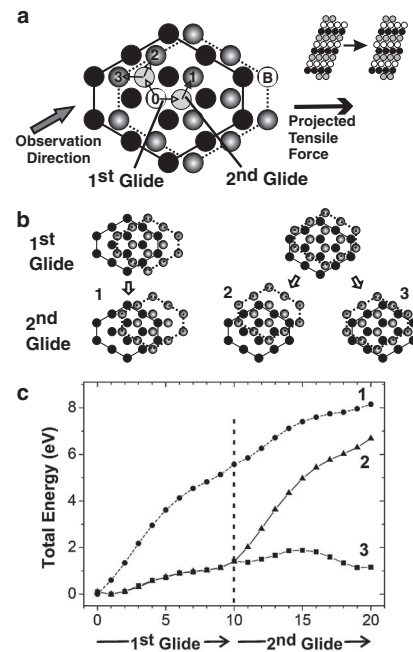
FIG. 4. Total energy changes associated with the generation of planar defects in an Au NR as shown in Fig. 2. (a) The (111) slip planes have a hexagonal shape; the sequential stacking of these planes (A, B, C) is represented by different colors (black, white, gray, respectively). To move from a B site (marked 0) into another B site, three different pathways are possible (final positions marked 1, 2, 3; there are three equivalent paths but moving downwards). The paths have been generated by two successive gliding steps. (b) To allow quick evaluation of the generated surface steps generated by the glides, the resulting structural configurations around the planar defect are displayed. (c) Total energy changes associated with the different pathways (calculations were performed considering 10 positions along each glide). In order to have a better visualization of the used structures and processes to obtain the barrier curves, see video 04, supplemental materials [12].
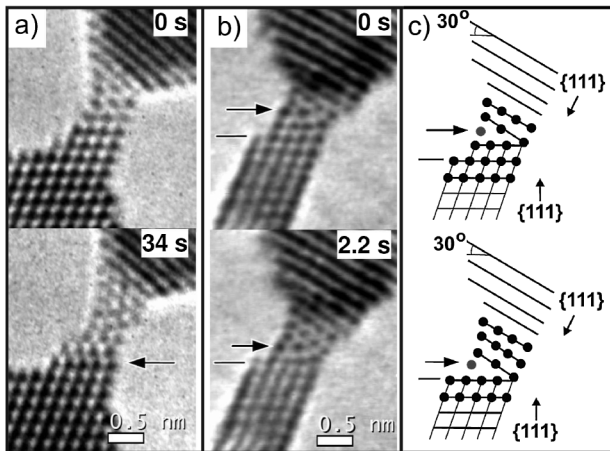

FIG. 3. Elongation of [110] Pt NRs: (a) 300 K; (b) 150 K. In contrast to Au systems, Pt rods of similar size display the formation of planar defects (arrowed in image 34 s) at room temperature. During the deformation at 150 K, the Pt rod displays a grain boundary [arrowed in (b)], which is moving down along the wire (a black bar serves as reference to visualize the boundary movement). A careful analysis of (b) reveals a boundary dislocation at the center of the wire. (c) Scheme of the atomic arrangement associated with Fig. 3(b); note that the misorientation between grains is about 30 degrees30° Atomic positions appear dark.

represents a driving force trying to spontaneously annihilate planar defects in the NR.

The curves show quite different energy dependence for each path. Pathway 1 (pure tensile deformation) exposes large surface steps [Fig. 4(b)] and then it has a high surface energy cost attaining ~8 eV at the final position. Paths 2 and 3 follow an identical first glide stage, whose energy cost is much lower than for path 1 [the induced surface step is smaller, see Figs. 4(b) and 4(c)]. This situation changes for the final second glide movement; a significant energy increase (~ 7 eV, and a much larger surface step) is attained at the end of path. We must emphasize that these total energy results indicate that the first slip along paths 2 or 3 should require lower energy to generate planar defects in the 1-nm-wide gold rods. This agrees with experiments [Fig. 1(b), 30.4 s], where the structural configuration containing a planar defect corresponds exactly to this particular situation [scheme in Fig. 2(b)]. Finally, path 3 (compression) represents the lowest energy cost deformation (softer response); then, our calculations predict a clear anisotropy mechanical behavior due to surface contributions. We must note that experimental studies of the deformation of gold pillars (200–900 nm in diameter) have revealed strong size effects; however, similar tensile or compressive flow stresses were observed [4,5,31]. This points to the essential role of size and shape for the mechanical properties of fcc metal rods with a diameter of a few nanometers.

Our results provide the first direct quantitative experimental information and energetic understanding for defects generation in 1-nm-wide gold rods. The relevant parameters to analyze nanoscale deformation mechanisms are surface energy, morphology (cross section and aspect ratio that determine how a defect will influence surface energy), defect blocking energy barrier (depends on material and system size), and, finally, the available thermal energy. For each kind of defect, material, and temperature, there is a threshold size for a particular defect to be considered an active nanoscale deformation mechanism. A nanosystem will behave as elastic until a defect with high enough blocking barrier can be nucleated. This study provides fundamental quantitative data to improve models and atomic potentials to be used in future temperature dependent simulations of the mechanical properties of nanostructures.

---

*dmugarte@ifi.unicamp.br

[1] C. Alloca and D. Smith, *Instrumentation and Metrology for Nanotechnology, Report of the National Nanotechnology Initiative* (available from http://www.nano.gov, 2005), Chap. 3.

[2] F. R. N. Nabarro, *Theory of Crystal Dislocations* (Dover, New York, 1987).

[3] W. D. Callister, *Materials Science and Engineering: An Introduction* (J. Wiley, New York, 2003).

[4] S. Brinckmann, J.-Y. Kim, and J. R. Greer, Phys. Rev. Lett. **100**, 155502 (2008).

[5] J. R. Greer, C. R. Weinberger, and W. Cai, Mater. Sci. Eng. A **493**, 21 (2008).

[6] J. H. Luo, F. F. Wu, J. Y. Huang, J. Q. Wang, and S. X. Mao, Phys. Rev. Lett. **104**, 215503 (2010).

[7] G. Rubio, N. Agraït, and S. Vieira, Phys. Rev. Lett. **76**, 2302 (1996).

[8] J. M. Buehler, *Atomistic Modeling of Materials Failure* (Springer, New York, 2008).

[9] *Atomistic Simulations of Mechanics of Nanostructures*, edited by H. Huang and H. Van Swygenhoven, MRS Bulletin (Materials Research Society, Pittsburgh, 2009), March issue.

[10] N. Agraït, A. L. Yeyati, and J. M. Ruittenbeek, Phys. Rep. **377**, 81 (2003).

[11] D. H. Warner, W. A. Curtin, and S. Qu, Nature Mater. **6**, 876 (2007).

[12] See supplemental material at http://link.aps.org/supplemental/10.1103/PhysRevLett.106.055501 for movies of the structural evolution of nanowire under stretching and an animated cartoon sequence of the structures used to generate the curves presented in Fig. 4.

[13] Y. Kondo and K. Takayanagi, Phys. Rev. Lett. **79**, 3455 (1997).

[14] H. Onishi, Y. Kondo, and K. Takayanagi, Nature (London) **395**, 780 (1998).

[15] D. Erts, H. Olin, L. Ryen, E. Olsson, and A. Thölén, Phys. Rev. B **61**, 12725 (2000).

[16] B. Peng *et al.*, Nature Nanotech. **3**, 626 (2008).

[17] T. Kizuka, Phys. Rev. B **77**, 155401 (2008).

[18] Y. Kurui, Y. Oshima, M. Okamoto, and K. Takayanagi, Phys. Rev. B **79**, 165414 (2009).

[19] V. Rodrigues, T. Fuhrer, and D. Ugarte, Phys. Rev. Lett. **85**, 4124 (2000).

[20] A. I. Yanson *et al.*, Nature (London) **395**, 783 (1998).

[21] U. Landman, W. D. Luedtke, N. A. Burnham, and R. J. Colton, Science **248**, 454 (1990).

[22] S. V. Bobylev and I. A. Ovid'ko, Phys. Rev. Lett. **103**, 135501 (2009).

[23] L. D. Marks, Rep. Prog. Phys. **57**, 603 (1994).

[24] V. Rodrigues and D. Ugarte, *Nanowires and Nanobelts*, edited by Z. L. Wang (Kluwer Academic Publishers, Boston, 2003), Vol. 1, Ch. 6.

[25] J. R. Rice, J. Mech. Phys. Solids **40**, 239 (1992).

[26] E. B. Tadmor and S. Hai, J. Mech. Phys. Solids **51**, 765 (2003).

[27] M. J. Mehl, D. A. Papaconstantopoulos, N. Kioussis, and M. Herbranson, Phys. Rev. B **61**, 4894 (2000).

[28] H. Van Swygenhoven, P. M. Derlet, and A. G. Froseth, Nature Mater. **3**, 399 (2004).

[29] L. Sun, A. V. Krasheninnikov, T. Ahlgren, K. Nordlund, and F. Banhart, Phys. Rev. Lett. **101**, 156101 (2008).

[30] D. Sánches-Portal, P. Ordejón, E. Artacho, and J. M. Soler, Int. J. Quantum Chem. **65**, 453 (1997).

[31] J.-Y. Kim and J. R. Greer, Acta Mater. **57**, 5245 (2009).